

Bayesian inference on isospin splitting of nucleon effective mass from giant resonances in $^{208}\text{Pb}^*$

Zhen Zhang(张振)^{1†} Xue-Bin Feng(冯学彬)¹ Lie-Wen Chen(陈列文)^{2‡}

¹Sino-French Institute of Nuclear Engineering and Technology, Sun Yat-sen University, Zhuhai 519082, China

²School of Physics and Astronomy, Shanghai Key Laboratory for Particle Physics and Cosmology, and Key Laboratory for Particle Astrophysics and Cosmology (MOE), Shanghai Jiao Tong University, Shanghai 200240, China

Abstract: From a Bayesian analysis of the electric dipole polarizability, the constrained energy of isovector giant dipole resonance, the peak energy of isoscalar giant quadrupole resonance, and the constrained energy of isoscalar giant monopole resonance in ^{208}Pb , we extract the isoscalar and isovector effective masses in nuclear matter at saturation density ρ_0 as $m_{s,0}^*/m = 0.87^{+0.04}_{-0.04}$ and $m_{v,0}^*/m = 0.78^{+0.06}_{-0.05}$, respectively, at 90% confidence level. The constraints obtained on $m_{s,0}^*$ and $m_{v,0}^*$ lead to a positive isospin splitting of nucleon effective mass in asymmetric nuclear matter of isospin asymmetry δ at ρ_0 as $m_{n-p}^*/m = (0.20^{+0.15}_{-0.14})\delta$. In addition, the symmetry energy at the subsaturation density $\rho^* = 0.05 \text{ fm}^{-3}$ is determined to be $E_{\text{sym}}(\rho^*) = 16.7 \pm 1.3 \text{ MeV}$ at 90% confidence level.

Keywords: nucleon effective mass, isospin splitting of nucleon effective mass, symmetry energy, nuclear giant resonance, Bayesian analysis

DOI: 10.1088/1674-1137/abf428

I. INTRODUCTION

The nucleon effective mass, which characterizes the momentum or energy dependence of a single nucleon potential in a nuclear medium, is crucial in nuclear physics and astrophysics [1-5]. While various types of nucleon effective masses have been defined in nonrelativistic and relativistic approaches [2-7], in this study, we focus on the total effective mass normally used in the nonrelativistic approach. In asymmetric nuclear matter, effective masses of neutrons and protons, i.e., m_n^* and m_p^* , respectively, may be different owing to the momentum dependence of the symmetry potential. The difference $m_{n-p}^* \equiv m_n^* - m_p^*$ is the so-called isospin splitting of nucleon effective mass, which plays an important role in many physical phenomena and questions in nuclear physics, astrophysics, and cosmology [4, 5]. For example, m_{n-p}^* affects the isospin dynamics in heavy-ion collisions [8-15], thermodynamic properties of asymmetric nuclear matter [16-18], and cooling of neutron stars [19].

Owing to the limited isospin asymmetry in normal nuclei, the accurate determination of m_{n-p}^* is difficult. Even the sign of m_{n-p}^* remains a debated issue. For example, $m_{n-p}^* > 0$ in neutron-rich matter at the nuclear saturation density $\rho_0 \approx 0.16 \text{ fm}^{-3}$ is favored by optical model

analyses of nucleon-nucleus scattering data [20, 21], Skyrme energy density functional (EDF) [22] and transport model [23] analyses of nuclear giant resonances, Brueckner-Hartree-Fock calculations [24-27], chiral effective theory [28-30], and an analysis of various constraints on the magnitude and density slope of symmetry energy [31]; in contrast, transport model analyses on single and/or double n/p ratio in heavy-ion collisions [32, 33] (see Ref. [34]) and an energy density functional study on nuclear electric dipole polarizability [35] lead to opposite conclusions.

Understanding these contradictive results and eventually determining the isospin splitting of nucleon effective mass require not only the improvement of both theoretical models/calculations and experimental measurements but also more sophisticated analysis approaches to quantifying the model uncertainties based on given experimental measurements. The latter is a quite general issue in nuclear theory: owing to the lack of a well-settled *ab initio* starting point, a considerable number of effective theories or models have been developed with parameters determined by fitting empirical knowledge or experimental data [36]. Over the past decade, various statistical approaches, e.g., covariance analysis [37, 38], Bayesian analysis [39-46], and bootstrap method [47, 48], were in-

Received 8 March 2021; Accepted 1 April 2021; Published online 26 April 2021

* Supported in part by the National Natural Science Foundation of China (11905302, 11625521) and National SKA Program of China (2020SKA0120300)

[†] E-mail: zhangzh275@mail.sysu.edu.cn, Corresponding author

[‡] E-mail: lwchen@sjtu.edu.cn, Corresponding author

©2021 Chinese Physical Society and the Institute of High Energy Physics of the Chinese Academy of Sciences and the Institute of Modern Physics of the Chinese Academy of Sciences and IOP Publishing Ltd

roduced in nuclear physics studies to quantify uncertainties and evaluate correlations of model parameters. Among them, the Bayesian inference method has been accepted as a powerful statistical approach and is extensively used in various areas of nuclear physics. For a recent review on Bayesian analysis and its application to nuclear structure study, please refer to Ref. [46].

In a previous study of ours [22], we extracted the isospin splitting of nucleon effective mass from the isovector giant dipole resonance (IVGDR) and isocalar giant quadrupole resonance (ISGQR) of ^{208}Pb based on random phase approximation (RPA) calculations using a number of representative Skyrme interactions. However, some factors in the analysis, e.g., the choice of Skyrme interactions and the previously assumed linear relations $1/E_{\text{GQR}}^2 - m_{s,0}^*$, could affect the conclusions, and the statistical meaning of the obtained uncertainties are therefore unclear. In the present study, within the framework of Skyrme energy density functional theory and random phase approximation approach, we employed the Bayesian inference method to extract the isospin splitting of nucleon effective mass from the electric dipole polarizability [49, 50], the constrained energy in IVGDR [51], and the ISGQR peak energy [52] in ^{208}Pb . The binding energy [53], charge radius [54], constrained energy of isocalar giant monopole resonance (ISGMR) [55], and neutron $3p_{1/2} - 3p_{3/2}$ energy splitting [56] of ^{208}Pb were also included in the analysis to guarantee that the energy density functional can always reasonably describe the ground state and collective excitation state of ^{208}Pb . The isoscalar and isovector effective masses and the neutron-proton effective mass splitting at saturation density, together with the symmetry energy at the subsaturation density $\rho^* = 0.05 \text{ fm}^{-3}$, were extracted from the Bayesian analysis.

The paper is organized as follows. In Sec. II, we introduce the theoretical models and statistical approaches used in this study. In the next section, we present the results for the uncertainties of model parameters, the isospin splitting of nucleon effective mass at ρ_0 , and the symmetry energy at $\rho^* = 0.05 \text{ fm}^{-3}$. Finally, we draw conclusions in Sec. IV.

II. MODEL AND METHOD

A. Nucleon effective mass in Skyrme energy density functional

As in Ref. [22], we studied the nucleon effective mass within the standard Skyrme energy density functional based on the conventional Skyrme interaction:

$$v(\mathbf{r}_1, \mathbf{r}_2) = t_0(1 + x_0 P_\sigma) \delta(\mathbf{r}_1 - \mathbf{r}_2) + \frac{1}{2} t_1(1 + x_1 P_\sigma) [\mathbf{k}'^2 \delta(\mathbf{r}_1 - \mathbf{r}_2) + \text{c.c.}]$$

$$+ t_2(1 + x_2 P_\sigma) \mathbf{k}' \cdot \delta(\mathbf{r}_1 - \mathbf{r}_2) \mathbf{k} + \frac{1}{6} t_3(1 + x_3 P_\sigma) \rho^\alpha \left(\frac{\mathbf{r}_1 + \mathbf{r}_2}{2} \right) \delta(\mathbf{r}_1 - \mathbf{r}_2) + i W_0 (\boldsymbol{\sigma}_1 + \boldsymbol{\sigma}_2) \cdot [\mathbf{k}' \times \delta(\mathbf{r}_1 - \mathbf{r}_2) \mathbf{k}]. \quad (1)$$

Here, $\boldsymbol{\sigma}_i$ is the Pauli spin operator, $P_\sigma = (1 + \boldsymbol{\sigma}_1 \cdot \boldsymbol{\sigma}_2)/2$ is the spin-exchange operator, $\mathbf{k} = -i(\nabla_1 - \nabla_2)/2$ is the relative momentum operator, and \mathbf{k}' is the conjugate operator of \mathbf{k} acting on the left.

Within the framework of Skyrme energy density functional, the nine parameters $t_0 - t_3$, $x_0 - x_3$, and α of the Skyrme interaction can be expressed in terms of nine macroscopic quantities (pseudo-observables): the nuclear saturation density ρ_0 , the energy per particle of symmetric nuclear matter $E_0(\rho_0)$, the incompressibility K_0 , the isocalar effective mass $m_{s,0}^*$ at ρ_0 , the isovector effective mass $m_{v,0}^*$ at ρ_0 , the gradient coefficient G_S , the symmetry-gradient coefficient G_V , and the magnitude $E_{\text{sym}}(\rho_0)$ and density slope L of the nuclear symmetry energy at ρ_0 [57-59]. The detailed analytical expressions can be found in Refs. [57, 58]. Given that these nine macroscopic quantities have clear physical meaning and available empirical ranges, we used them as model parameters in the Bayesian analysis. Consequently, our model has the following 10 parameters:

$$\mathbf{p} = \{\rho_0, E_0(\rho_0), K_0, E_{\text{sym}}(\rho_0), L, G_S, G_V, W_0, m_{s,0}^*, m_{v,0}^*\}. \quad (2)$$

In terms of the Skyrme parameters $t_0 \sim t_3$ and $x_0 \sim x_3$, the nucleon effective mass in asymmetric nuclear matter with density ρ and isospin asymmetry δ can be expressed as [60]

$$\frac{\hbar^2}{2m_q^*(\rho, \delta)} = \frac{\hbar^2}{2m} + \frac{1}{4} t_1 \left[\left(1 + \frac{1}{2} x_1 \right) \rho - \left(\frac{1}{2} + x_1 \right) \rho_q \right] + \frac{1}{4} t_2 \left[\left(1 + \frac{1}{2} x_2 \right) \rho + \left(\frac{1}{2} + x_2 \right) \rho_q \right]. \quad (3)$$

The well-known isocalar and isovector effective masses, i.e., m_s^* and m_v^* , which are respectively defined as the proton (neutron) effective mass in symmetric nuclear matter and pure neutron (proton) matter, are then expressed as [60]

$$\frac{\hbar^2}{2m_s^*(\rho)} = \frac{\hbar^2}{2m} + \frac{3}{16} t_1 \rho + \frac{1}{16} t_2 (4x_2 + 5) \rho, \quad (4)$$

$$\frac{\hbar^2}{2m_v^*(\rho)} = \frac{\hbar^2}{2m} + \frac{1}{8} t_1 (x_1 + 2) \rho + \frac{1}{8} t_2 (x_2 + 2) \rho. \quad (5)$$

Once given m_s^* and m_v^* , the isospin splitting of nucleon

effective mass can be obtained as [61]

$$\begin{aligned} m_{n-p}^*(\rho, \delta) &\equiv \frac{m_n^* - m_p^*}{m} = 2 \frac{m_s^*}{m} \sum_{n=1}^{\infty} \left(\frac{m_s^* - m_v^*}{m_v^*} \delta \right)^{2n-1} \\ &= \sum_{n=1}^{\infty} \Delta m_{2n-1}^*(\rho) \delta^{2n-1}, \end{aligned} \quad (6)$$

with the isospin splitting coefficients $\Delta m_{2n-1}^*(\rho)$ expressed as

$$\Delta m_{2n-1}^*(\rho) = 2 \frac{m_s^*}{m} \left(\frac{m_s^*}{m_v^*} - 1 \right)^{2n-1}. \quad (7)$$

In the following, we use Δm_1^* to indicate the linear isospin splitting coefficient at the saturation density ρ_0 .

B. Nuclear giant resonances

Nuclear giant resonances are usually studied using the random phase approximation (RPA) approach [62]. For a given excitation operator \hat{F}_{JM} , the strength function is calculated as

$$S(E) = \sum_{\nu} |\langle \nu | \hat{F}_{JM} | \bar{0} \rangle|^2 \delta(E - E_{\nu}), \quad (8)$$

with E_{ν} denoting the energy of the RPA excitation state $|\nu\rangle$; the moments m_k of strength function (sum rules) are usually evaluated as follows:

$$m_k = \int dE E^k S(E) = \sum_{\nu} |\langle \nu | \hat{F}_{JM} | \bar{0} \rangle|^2 E_{\nu}^k. \quad (9)$$

For the ISGMR, IVGDR, and ISGQR studied here, the excitation operators are defined as follows:

$$\hat{F}_0^{\text{IS}} = \sum_i^A r_i^2 \quad (10)$$

$$\hat{F}_{1M}^{\text{IV}} = \frac{N}{A} \sum_{i=1}^Z r_i Y_{1M}(\hat{r}_i) - \frac{Z}{A} \sum_{i=1}^N r_i Y_{1M}(\hat{r}_i), \quad (11)$$

$$\hat{F}_{2M}^{\text{IS}} = \sum_{i=1}^A r_i^2 Y_{2M}(\hat{r}_i), \quad (12)$$

where Z , N , and A are proton, neutron, and mass number, respectively; r_i is the nucleon's radial coordinate; $Y_{1M}(\hat{r}_i)$ and $Y_{2M}(\hat{r}_i)$ are the corresponding spherical harmonic functions.

Particularly, in linear response theory, the inverse en-

ergy weighted sum rule can also be extracted from the constrained Hartree-Fock (CHF) approach [63, 64]:

$$m_{-1} = - \frac{1}{2} \left. \frac{d^2 \langle \lambda | \mathcal{H} | \lambda \rangle}{d\lambda^2} \right|_{\lambda=0}, \quad (13)$$

where $|\lambda\rangle$ is the ground-state for the nuclear system Hamilton \mathcal{H} constrained by the field $\lambda \hat{F}_J$.

The energy of isoscalar giant monopole resonance (GMR), i.e., the breathing mode, is an important probe of the incompressibility in nuclear matter. It can be evaluated according to the constrained approximation [65] as

$$E_{\text{GMR}} = \sqrt{\frac{m_1(\text{GMR})}{m_{-1}(\text{GMR})}}, \quad (14)$$

where the energy weighted sum rule m_1 of ISGMR is related to the ground-state rms radius $\langle r^2 \rangle$ by [66]

$$m_1(\text{GMR}) = 2 \frac{\hbar^2}{m} A \langle r^2 \rangle. \quad (15)$$

Therefore, we calculated E_{GMR} by using the CHF method for computational efficiency.

Concerning the isovector giant dipole resonance, we considered two observables, namely the electric dipole polarizability α_{D} and the constrained energy $E_{\text{GDR}} \equiv \sqrt{m_1/m_{-1}}$. Note that α_{D} in ^{208}Pb probes the symmetry energy at approximately $\rho_0/3$ [61] and is therefore sensitive to both the magnitude and density slope of the symmetry energy at saturation density [67]. It is related to the inverse energy-weighted sum rule in the IVGDR through

$$\alpha_{\text{D}} = \frac{8\pi}{9} e^2 m_{-1}(\text{GDR}). \quad (16)$$

Meanwhile, the energy weighted sum rule m_1 of IVGDR is related to the isovector effective mass at saturation density $m_{v,0}^*$ via [22, 62]

$$m_1(\text{GDR}) = \frac{9}{4\pi} \frac{\hbar^2}{2m} \frac{NZ}{A} (1 + \kappa) \approx \frac{9\hbar^2}{8\pi} \frac{NZ}{A} \frac{1}{m_{v,0}^*}, \quad (17)$$

where κ is the well-known Thomas-Reiche-Kuhn sum rule enhancement. One then has approximately

$$E_{\text{GDR}}^2 \propto \frac{1}{m_{v,0}^* \alpha_{\text{D}}}, \quad (18)$$

which suggests that E_{GDR} is negatively correlated with respect to $m_{v,0}^*$.

It is well known that the excitation energy of isoscalar giant quadrupole resonance is sensitive to the isoscalar effective mass at saturation density. For example, in the harmonic oscillator model, the ISGQR energy is [52, 66]

$$E_{\text{GQR}} = \sqrt{\frac{2m}{m_{s,0}^*}} \hbar\omega_0 \quad (19)$$

with $\hbar\omega_0$ denoting the frequency of the harmonic oscillator. In the present study, we set E_{GQR} as the peak energy of the response function obtained from RPA calculations. To obtain a continuous response function, the discrete RPA results were smeared out with Lorentzian functions. The width of Lorentzian functions was set to be 3 MeV to reproduce an experimental width of ~ 3 MeV for ISGQR in ^{208}Pb .

C. Bayesian analysis

Bayesian analysis has been widely accepted as a powerful statistical approach to quantifying the uncertainties and evaluating the correlations of model parameters as well as making predictions with a certain confidence level according to experimental measurements and empirical knowledge [39-46]. In this study, we employed the MADAI package [68] to conduct Bayesian analysis based on Gaussian process emulators. For further details on this statistical approach, please refer to, e.g., Ref. [40].

According to Bayes' theorem, the posterior probability distribution of model parameters \mathbf{p} (which we are seeking for), with given experimental measurements \mathcal{O}^{exp} for a set of observables \mathcal{O} can be evaluated as

$$P(\mathbf{p}|\mathcal{M}, \mathcal{O}^{\text{exp}}) = \frac{P(\mathcal{M}, \mathcal{O}^{\text{exp}} | \mathbf{p})P(\mathbf{p})}{\int P(\mathcal{M}, \mathcal{O}^{\text{exp}} | \mathbf{p})P(\mathbf{p})d\mathbf{p}}, \quad (20)$$

where \mathcal{M} is the given model, $P(\mathbf{p})$ is the prior probability of model parameters \mathbf{p} before being confronted with the experimental measurements \mathcal{O}^{exp} , and $P(\mathcal{M}, \mathcal{O}^{\text{exp}}|\mathbf{p})$ denotes the likelihood or the conditional probability of observing \mathcal{O}^{exp} with given model \mathcal{M} predictions at \mathbf{p} . The posterior univariate distribution of a single model parameter p_i is given by

$$P(p_i|\mathcal{M}, \mathcal{O}^{\text{exp}}) = \frac{\int P(\mathbf{p}|\mathcal{M}, \mathcal{O}^{\text{exp}})d\prod_{j \neq i} p_j}{\int P(\mathbf{p}|\mathcal{M}, \mathcal{O}^{\text{exp}})d\prod_j p_j}, \quad (21)$$

and the correlated bivariate distribution of two parameters p_i and p_j is given by

$$P[(p_i, p_j)|\mathcal{M}, \mathcal{O}^{\text{exp}}] = \frac{\int P(\mathbf{p}|\mathcal{M}, \mathcal{O}^{\text{exp}})d\prod_{k \neq i, j} p_k}{\int P(\mathbf{p}|\mathcal{M}, \mathcal{O}^{\text{exp}})d\prod_k p_k}. \quad (22)$$

From the univariate distribution, the mean value of p_i can be calculated as

$$\langle p_i \rangle = \int p_i P(p_i|\mathcal{M}, \mathcal{O}^{\text{exp}})dp_i. \quad (23)$$

The confidence interval of p_i at a confidence level $1 - \alpha$ is normally obtained as the interval between the $(50\alpha)^{\text{th}}$ and $(100 - 50\alpha)^{\text{th}}$ percentile of the posterior univariate distribution. Particularly, the median value U_{p_i} of p_i is defined as the 50th percentile, i.e.,

$$\int_{-\infty}^{U_{p_i}} P(p_i|\mathcal{M}, \mathcal{O}^{\text{exp}})dp_i = 0.5. \quad (24)$$

Concerning the prior distribution, we assumed that the ten parameters are uniformly distributed in the empirical ranges listed in Table 1. It can be concluded from Eq. (20) that the posterior distribution is determined by the combination of the prior distribution and the likelihood function, which depends on the experimental measurement for an observable. Therefore, the prior distribution is critical in the Bayesian analysis and can significantly affect the extracted constraints. Nevertheless, in the present study, owing to the relatively poor knowledge on $m_{s,0}^*$ and $m_{v,0}^*$ in the Skyrme EDF, we assumed large prior ranges for $m_{s,0}^*$ and $m_{v,0}^*$. Consequently, the constraints on nucleon effective masses were mainly due to the giant resonance observables. Narrowing the prior ranges for all the parameters by 20% slightly reduced the posterior uncertainties of the isospin splitting of nucleon effective mass by a small percentage.

Table 1. Prior ranges of the ten parameters used.

Quantity	lower limit	upper limit
ρ_0/fm^{-3}	0.155	0.165
E_0/MeV	-16.5	-15.5
K_0/MeV	210.0	250.0
$E_{\text{sym}}(\rho_0)/\text{MeV}$	29.0	35.0
L/MeV	20.0	120.0
$G_S/(\text{MeV} \cdot \text{fm}^5)$	110.0	170.0
$G_V/(\text{MeV} \cdot \text{fm}^5)$	-70.0	70.0
$W_0/(\text{MeV} \cdot \text{fm}^5)$	110.0	140.0
$m_{s,0}^*/m$	0.7	1.0
$m_{v,0}^*/m$	0.6	0.9

The likelihood function was set to be the commonly used Gaussian form

$$P(\mathcal{M}, O_i^{\text{exp}} | \mathbf{p}) \propto \exp \left\{ - \sum_i \frac{[O_i(\mathbf{p}) - O_i^{\text{exp}}]^2}{2\sigma_i^2} \right\}, \quad (25)$$

where $O_i(\mathbf{p})$ is the model prediction for an observable at given points \mathbf{p} , O_i^{exp} is the corresponding experimental measurement, and σ_i is the uncertainty or the width of likelihood function. For a given parameter set \mathbf{p} , we calculated the following seven observables in ^{208}Pb from Hartree-Fock, CHF, and RPA calculations: the electric dipole polarizability α_D [49, 50], the IVGDR constrained energy E_{GDR} [51], the ISGQR peak energy E_{GQR} [52], the binding energy E_B [53], the charge radius r_C [54], the breathing mode energy E_{GMR} [55], and the neutron $3p_{1/2} - 3p_{3/2}$ energy level splitting ϵ_{ls} [56]. The experimental values for these seven observables together with the assigned uncertainties are listed in Table 2. Regard-

Table 2. Experimental values and uncertainties used for the binding energy E_B [53], charge radius r_C [54], breathing mode energy E_{GMR} [55], neutron $3p_{1/2} - 3p_{3/2}$ energy level splitting ϵ_{ls} [56], electric dipole polarizability α_D [49, 50], IVGDR constrained energy [51], and ISGQR peak energy [52] in ^{208}Pb .

	value	σ
E_B/MeV	-1363.43	0.5
r_C/fm	5.5012	0.01
$E_{\text{GMR}}/\text{MeV}$	13.5	0.1
ϵ_{ls}/MeV	0.89	0.09
α_D/fm^3	19.6	0.6
$E_{\text{GDR}}/\text{MeV}$	13.46	0.1
$E_{\text{GQR}}/\text{MeV}$	10.9	0.1

ing α_D and E_{GMR} , σ_i were set to be their experimental uncertainties given in Refs. [49] and [55]; for proper determination of E_B , r_C , ϵ_{ls} , and E_{GDR} , we assigned them artificial 1σ errors of 0.5 MeV, 0.01 fm, 0.09 MeV, and 0.1 MeV, respectively; concerning the experimental value and uncertainty of E_{GQR} , we used the weighted average of experimental measurements, i.e., 10.9 ± 0.1 MeV, reported in Ref. [52]. Note that decreasing the artificial errors of E_B , r_C , ϵ_{ls} , and E_{GDR} by half slightly reduced the posterior uncertainty of Δm_1^* by approximately 7% and did not affect the constraint on the symmetry energy at subsaturation density $\rho^* = 0.05 \text{ fm}^{-3}$.

According to the prior distribution and defined likelihood function, the Markov chain Monte Carlo (MCMC) process using Metropolis-Hastings algorithm was performed to evaluate the posterior distributions of model parameters. For the 10-dimensional parameter space in this study, a great deal of MCMC steps would be needed to extract posterior distributions. Thus, theoretical calculations for all the MCMC steps are infeasible. Instead, in this study, we first sampled a number of parameter sets in the designed parameter space, and trained Gaussian process (GP) emulators [69] using the model predictions with the sampled parameter sets. The obtained GPs provided fast interpolators and were used to evaluate the likelihood function in each MCMC step.

III. RESULTS AND DISCUSSIONS

We first generated 2500 parameter sets using the maximin Latin cube sampling method [70]. Twenty-four of them were located near the edge of the allowed parameter space and led to numerical instability in Hartree-Fock (HF) or RPA calculations. Therefore, we discarded these twenty-four parameter sets and used the remaining 2476 parameter sets in HF, CHF, and RPA calculations to obtain the training data for Gaussian emulators.

Results from these 2476 training points pointed out

Table 3. Best value, mean, median, and confidence intervals of the model parameters from MCMC sampling.

	best	mean	median	68.3% C.I.	90% C.I.	95.4% C.I.
ρ_0/fm^{-3}	0.1597	0.1612	0.1613	0.1589 ~ 0.1635	0.1577 ~ 0.1644	0.1570 ~ 0.1647
E_0/MeV	-16.04	-16.10	-16.10	-16.34 ~ -15.87	-16.44 ~ -15.78	-16.47 ~ -15.74
K_0/MeV	224.6	223.5	223.4	219.4 ~ 227.6	216.9 ~ 230.3	215.6 ~ 231.8
$E_{\text{sym}}(\rho_0)/\text{MeV}$	34.4	32.7	33.0	30.9 ~ 34.4	29.9 ~ 34.8	29.5 ~ 34.9
$L(\rho_0)/\text{MeV}$	48.8	40.3	40.4	27.9 ~ 51.9	22.8 ~ 58.1	21.4 ~ 61.1
$G_S/(\text{MeV} \cdot \text{fm}^5)$	125.7	135.5	135.1	118.2 ~ 152.5	112.7 ~ 160.3	111.2 ~ 163.5
$G_V/(\text{MeV} \cdot \text{fm}^5)$	65.0	-1.6	-3.1	-50.9 ~ 49.5	-64.1 ~ 63.9	-67.3 ~ 67.3
$W_0/(\text{MeV} \cdot \text{fm}^5)$	111.6	118.4	117.0	112.0 ~ 125.1	110.6 ~ 131.4	110.3 ~ 134.7
$m_{s,0}^*/m$	0.88	0.87	0.87	0.84 ~ 0.89	0.83 ~ 0.91	0.82 ~ 0.92
$m_{v,0}^*/m$	0.78	0.78	0.78	0.75 ~ 0.81	0.73 ~ 0.84	0.72 ~ 0.85

ρ_0	-0.054	0.052	0.146	0.166	-0.662	0.072	0.266
E_0	0.025	-0.009	-0.040	0.767	0.024	-0.123	-0.063
K_0	-0.063	0.062	0.089	0.174	-0.246	0.883	0.094
$E_{\text{sym}}(\rho_0)$	-0.291	0.253	-0.093	0.178	-0.024	-0.156	-0.101
L	0.889	-0.807	0.024	-0.233	-0.194	0.059	-0.189
G_S	0.180	-0.186	-0.199	0.463	0.568	-0.323	-0.236
G_V	0.072	-0.050	0.066	-0.025	-0.066	0.045	0.048
W_0	-0.019	0.019	0.094	-0.074	-0.168	0.067	0.719
$m_{s,0}^*$	0.127	-0.122	-0.923	0.254	0.262	-0.204	-0.542
$m_{v,0}^*$	-0.019	-0.474	0.118	-0.025	0.016	0.032	0.067
	α_D	E_{GDR}	E_{GQR}	E_B	r_C	E_{GMR}	ϵ_{ts}

Fig. 1. (color online) Visualization of the Pearson correlation coefficients among model parameters and observables from the training data. The numerical values of correlation coefficients are annotated and color-coded: darker red indicates greater positive values and darker blue indicates greater negative values.

possible correlations between observables and model parameters. Fig. 1 shows the Pearson correlation coefficients among model parameters and the seven selected observables obtained from the training data. In Fig. 1, darker red indicates larger positive values, that is, stronger positive correlation, whereas darker blue indicates greater negative values, that is, stronger negative correlation. One can expect that parameters strongly correlated with the chosen observables are more likely to be constrained. Particularly, note that the correlations among observables in nuclear giant resonances and model parameters are clearly consistent with the empirical knowledge introduced in Section II B: α_D is positively (negatively) correlated with L [$E_{\text{sym}}(\rho_0)$] because it is mostly sensitive to the symmetry energy at $\rho^* = 0.05 \text{ fm}^{-3}$ [61]; E_{GDR} is negatively correlated with both $m_{v,0}^*$ and L but positively with $E_{\text{sym}}(\rho_0)$, which can be understood from Eq. (18) and the dependence of α_D on L and $E_{\text{sym}}(\rho_0)$; E_{GQR} presents a strong negative correlation with $m_{s,0}^*$ [see Eq. (19)]; E_{GMR} is mostly sensitive to the incompressibility, denoted as K_0 . Meanwhile, G_V is weakly correlated with all observables; therefore, it could not be well constrained in the present analysis.

Based on the training data, Gaussian process emulators were tuned to quickly predict the model output for the

MCMC process. With the help of GPs, we first ran 10^6 burn-in MCMC steps to allow the chain to reach equilibrium, and then generated 10^7 points in the parameter space via MCMC sampling. The posterior distributions of model parameters were then extracted from the 10^7 samples; they are shown in Fig. 2. The lower-left panels show bivariate scatter histograms of the MCMC samples; the diagonal ones present the univariate posterior distribution of the model parameters; the solid, dashed, and dotted lines in the upper-right panels enclose 68.3%, 90%, and 95.4% confidence regions, respectively. Fig. 2 intuitively presents the uncertainties and correlations of the model parameters imposed by the experimental measurements for the chosen observables. Remarkably, K_0 , $m_{s,0}^*$, and $m_{v,0}^*$ are well constrained by the giant monopole, dipole, and quadrupole resonances, respectively. Another interesting feature is the strong positive correlation between $E_{\text{sym}}(\rho_0)$ and L , which can be understood by the fact that α_D is positively correlated with L but negatively correlated with $E_{\text{sym}}(\rho_0)$ (see Fig. 1). Similarly, the E_B datum leads to a negative E_0 - G_S correlation, whereas the r_C datum results in a positive ρ_0 - G_S correlation. Therefore, the combination of E_B and r_C leads to a negative ρ_0 - E_0 correlation.

To quantify the posterior distribution from Bayesian analysis, we listed in Table 3 the statistical quantities estimated from the MCMC samples, including the mean value, median value, and confidence intervals at 68.3%, 90%, and 95.4% confidence levels. The best value, i.e., the parameter set that gives the largest likelihood function, was also listed for reference. In particular, we obtained $m_{s,0}^*/m = 0.87^{+0.02}_{-0.03}$ and $m_{v,0}^*/m = 0.78^{+0.03}_{-0.03}$ at 68% confidence level, and $m_{s,0}^*/m = 0.87^{+0.04}_{-0.04}$ and $m_{v,0}^*/m = 0.78^{+0.06}_{-0.05}$ at 90% confidence level. These results are consistent with $m_{s,0}^* = 0.91 \pm 0.05$ and $m_{v,0}^*/m = 0.8 \pm 0.03$ extracted from the GDR and GQR in Ref. [22] using the conventional method. Note that, compared with a previous study of ours [22] in which a conventional analysis was carried out based only on 50 representative Skyrme EDFs, in the present study, we extracted the posterior distributions of model parameters from a very large number of parameter sets from MCMC sampling. Therefore, the uncertainties of model parameters were better evaluated, and the constraints obtained in the present study should be more reliable. The 90% confidence interval obtained for $m_{v,0}^*$ is also in very good agreement with the result of $0.79^{+0.06}_{-0.06}$ from a recent Bayesian analysis of giant dipole resonance in ^{208}Pb [45]. Note that, compared with the present study, the Bayesian analysis in Ref. [45] employed the same GDR data, but the MCMC process was based on fully self-consistent RPA calculations. Therefore, the consistence between the two results further confirms the reliability of Gaussian emulators as a fast surrogate of real model calculations.

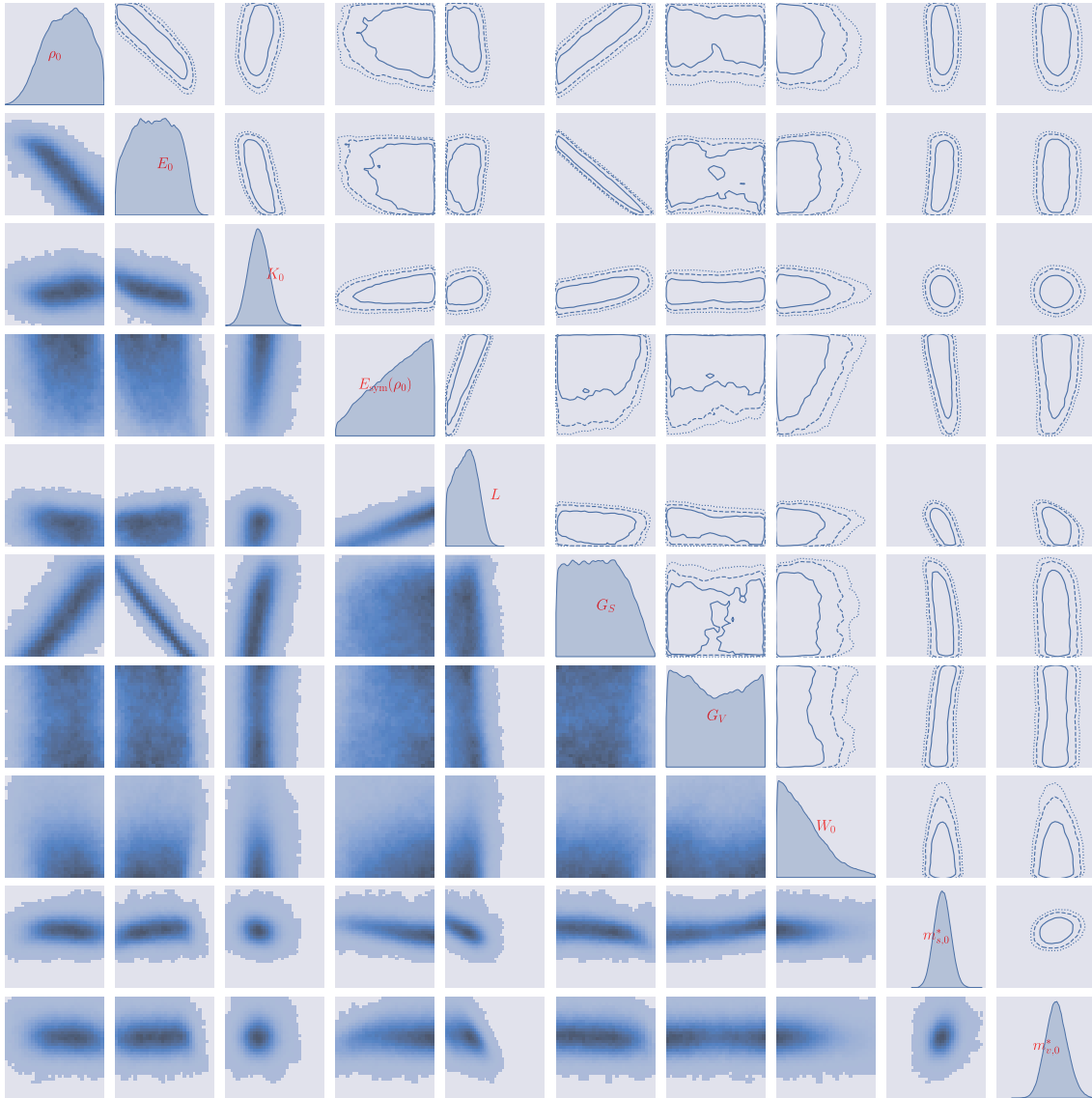


Fig. 2. (color online) Univariate and bivariate posterior distributions of the ten model parameters. The solid, dashed, and dotted lines in the upper-right panels enclose 68.3%, 90%, and 95.4% confidence regions, respectively; the diagonal plots show Gaussian kernel density estimations of the posterior marginal distribution for the respective parameters; the lower-left panels show scatter histograms of MCMC samples. The ranges of variations of the ten parameters are the prior ranges listed in Table 1.

Fig. 3 further shows the posterior bivariate and univariate distributions of the symmetry energy at $\rho^* = 0.05 \text{ fm}^{-3}$ and the linear isospin splitting coefficient Δm_1^* at ρ_0 . Given the approximate relations $E_{\text{sym}}(\rho^*) \propto 1/\alpha_{\text{D}}$ and $E_{\text{GDR}}^2 \propto (\alpha_{\text{D}} m_{v,0}^*)^{-1}$, the GDR data lead to positive correlation between $E_{\text{sym}}(\rho^*)$ and $m_{v,0}^*$. Therefore, Fig. 3 exhibits a negative $E_{\text{sym}}(\rho^*)$ - Δm_1^* correlation [see Eq. (7)]. The confidence intervals of $E_{\text{sym}}(\rho^*)$ and Δm_1^* can be extracted from their univariate distributions shown in Figs. 3(b) and (c). Specifically, we obtained $E_{\text{sym}}(\rho^*) = 16.7_{-0.8}^{+0.8} \text{ MeV}$ and $\Delta m_1^* = 0.20_{-0.09}^{+0.09}$ at 68.3% confidence level, and $E_{\text{sym}}(\rho^*) = 16.7_{-1.3}^{+1.3} \text{ MeV}$ and $\Delta m_1^* = 0.20_{-0.14}^{+0.15}$ at 90% confidence level. For the higher

order terms, we found, for example, that Δm_3^* is less than 0.01 at 90% confidence level and therefore can be neglected.

Within the uncertainties, the present constraint on Δm_1^* is consistent with the constraints $m_{n-p}^*/m = (0.32 \pm 0.15)\delta$ [21] and $m_{n-p}^*/m = (0.41 \pm 0.15)\delta$ [20] extracted from a global optical model analysis of nucleon-nucleus scattering data, and also agrees with $\Delta m_1^* = 0.27$ obtained by analyzing various constraints on the magnitude and density slope of the symmetry energy [31]. It is also consistent with the constraints from analyses of isovector GDR and isoscalar GQR with RPA calculations using Skyrme interactions [22] and the transport model using an improved isospin- and momentum-dependent interac-

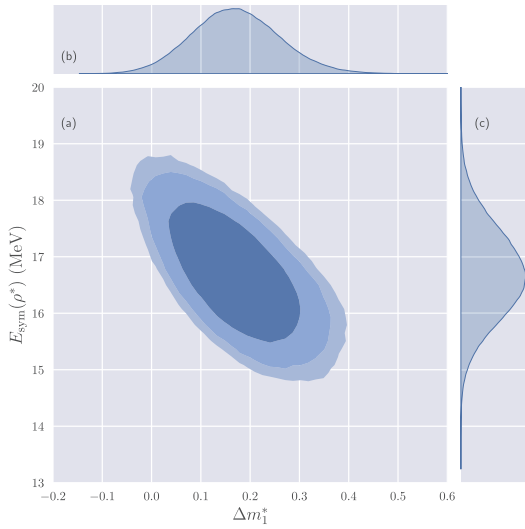


Fig. 3. (color online) Posterior bivariate (a) and univariate [(b) and (c)] distributions of $E_{\text{sym}}(\rho^*)$ at $\rho^* = 0.05 \text{ fm}^{-3}$, and linear isospin splitting coefficient Δm_1^* at ρ_0 . The shaded regions in window (a) indicate the 68.3%, 90%, and 95.4% confidence regions.

tion [23]. In addition, the present constraint $E_{\text{sym}}(\rho^*) = 16.7^{+1.3}_{-1.3} \text{ MeV}$ is consistent with the result $15.91 \pm 0.99 \text{ MeV}$ obtained in Ref. [61], in which the used experimental value of α_D in ^{208}Pb contains a non-negligible amount of contamination caused by quasideuteron excitations [55]. Subtracting the contribution of the quasideuteron effect will slightly enhance $E_{\text{sym}}(\rho^*)$, thereby improving the agreement with the results reported herein.

To end this section, we present the limitations of this study. We only focused on nuclear giant resonances in ^{208}Pb . However, $m_{v,0}^*$ from the GDR of ^{208}Pb is not consistent with the GDR in ^{16}O [71]. Describing the giant resonances simultaneously in light and heavy nuclei is still a challenge. Concerning the ambiguities in determining nucleon effective masses from nuclear giant reson-

ances, please refer to Ref. [5]. It is also worth mentioning that owing to the simple quadratic momentum dependence of the single-nucleon potential in Skyrme energy density functional, the nucleon effective mass is momentum independent and only has a simple density dependence [see Eq. (3)], which is not the case in microscopic many body theories, such as the chiral effective theory [29, 30]. The extended Skyrme pseudopotential [72-74] with higher order momentum-dependent terms may help to address the issues on isospin splitting of nucleon effective mass.

IV. CONCLUSIONS

Within the framework of Skyrme energy density functional and random phase approximation, we conducted Bayesian analysis for data on the ground and collective excitation states of ^{208}Pb to extract information on the nucleon effective mass and its isospin splitting. Our results indicate that the isoscalar effective mass $m_{s,0}^*/m$ exhibits a particularly strong correlation with the peak energy of isoscalar giant quadrupole resonance, and the isovector effective mass $m_{v,0}^*/m$ is correlated with the constrained energy of isovector giant dipole resonance. By including the constrained energy of the isoscalar monopole resonance, the peak energy of isoscalar giant quadrupole resonance, the electric dipole polarizability, and the constrained energy of the isovector giant dipole resonance in the analysis, we constrained the isoscalar and isovector effective masses and the isospin splitting of nucleon effective masses at saturation density as $m_{s,0}^*/m = 0.87^{+0.04}_{-0.04}$, $m_{v,0}^*/m = 0.78^{+0.06}_{-0.05}$, and $m_{n-p}^*/m = (0.20^{+0.15}_{-0.14})\delta$, respectively, at 90% confidence level. For a 68.3% (1σ) confidence level, the constraints become $m_{s,0}^*/m = 0.87^{+0.02}_{-0.03}$, $m_{v,0}^*/m = 0.78^{+0.03}_{-0.03}$, and $m_{n-p}^*/m = (0.20^{+0.09}_{-0.08})\delta$. In addition, the symmetry energy at the subsaturation density $\rho^* = 0.05 \text{ fm}^{-3}$ was constrained as $E_{\text{sym}}(\rho^*) = 16.7^{+0.8}_{-0.8} \text{ MeV}$ at 68.3% confidence level and $E_{\text{sym}}(\rho^*) = 16.7^{+1.3}_{-1.3} \text{ MeV}$ at 90% confidence level.

References

- [1] J. Jeukenne, A. Lejeune, and C. Mahaux, Phys. Rep. **25**, 83 (1976)
- [2] C. Mahaux, P. Bortignon, R. Broglia *et al.*, Phys. Rep. **120**, 1 (1985)
- [3] M. Jamion and C. Mahaux, Phys. Rev. C **40**, 354 (1989)
- [4] B.-A. Li and L.-W. Chen, Mod. Phys. Lett. A **30**, 1530010 (2015)
- [5] B. A. Li, B. J. Cai, L. W. Chen *et al.*, Prog. Part. Nucl. Phys. **99**, 29 (2018), arXiv:1801.01213
- [6] L. W. Chen, C. M. Ko, and B. A. Li, Phys. Rev. C **76**, 054316 (2007)
- [7] B. A. Li, L. W. Chen, and C. M. Ko, Phys. Rep. **464**, 113 (2008)
- [8] B.-A. Li, C. B. Das, S. Das Gupta *et al.*, Phys. Rev. C **69**, 011603 (2004)
- [9] B.-A. Li and L.-W. Chen, Phys. Rev. C **72**, 064611 (2005)
- [10] L.-W. Chen, C. M. Ko, and B.-A. Li, Phys. Rev. Lett. **94**, 032701 (2005)
- [11] J. Rizzo, M. Colonna, and M. D. Toro, Phys. Rev. C **72**, 064609 (2005)
- [12] V. Giordano, M. Colonna, M. Di Toro *et al.*, Phys. Rev. C **81**, 044611 (2010)
- [13] Z.-Q. Feng, Phys. Lett. B **707**, 83 (2012)
- [14] Y. Zhang, M. Tsang, Z. Li, and H. Liu, Phys. Lett. B **732**, 186 (2014)
- [15] W.-J. Xie and F.-S. Zhang, Phys. Lett. B **735**, 250 (2014)
- [16] B. Behera, T. R. Routray, and S. K. Tripathy, J. Phys. G **38**, 115104 (2011)

- [17] J. Xu, L.-W. Chen, and B.-A. Li, *Phys. Rev. C* **91**, 014611 (2015)
- [18] J. Xu, *Phys. Rev. C* **91**, 037601 (2015)
- [19] M. Baldo, G. F. Burgio, H.-J. Schulze *et al.*, *Phys. Rev. C* **89**, 048801 (2014)
- [20] X.-H. Li, W.-J. Guo, B.-A. Li *et al.*, *Phys. Lett. B* **743**, 408 (2015)
- [21] C. Xu, B.-A. Li, and L.-W. Chen, *Phys. Rev. C* **82**, 054607 (2010)
- [22] Z. Zhang and L. W. Chen, *Phys. Rev. C* **93**, 034335 (2016)
- [23] H.-Y. Kong, J. Xu, L.-W. Chen *et al.*, *Phys. Rev. C* **95**, 034324 (2017)
- [24] W. Zuo, I. Bombaci, and U. Lombardo, *Phys. Rev. C* **60**, 024605 (1999)
- [25] W. Zuo, L. G. Cao, B. A. Li *et al.*, *Phys. Rev. C* **72**, 014005 (2005)
- [26] Z.-Y. Ma, J. Rong, B.-Q. Chen *et al.*, *Phys. Lett. B* **604**, 170 (2004)
- [27] E. N. E. van Dalen, C. Fuchs, and A. Faessler, *Phys. Rev. Lett.* **95**, 022302 (2005)
- [28] Z. Zhang, Y. Lim, J. W. Holt, and C. M. Ko, *Phys. Lett. B* **777**, 73 (2018)
- [29] J. W. Holt, N. Kaiser, G. A. Miller *et al.*, *Phys. Rev. C* **88**, 024614 (2013)
- [30] J. W. Holt, N. Kaiser, and G. A. Miller, *Phys. Rev. C* **93**, 064603 (2016)
- [31] B. A. Li and X. Han, *Phys. Lett. B* **727**, 276 (2013)
- [32] D. D. S. Coupland, M. Youngs, Z. Chajecki *et al.*, *Phys. Rev. C* **94**, 011601 (2016)
- [33] P. Morfouace, C. Y. Tsang, Y. Zhang *et al.*, *Phys. Lett. B* **799**, 135045 (2019)
- [34] H.-Y. Kong, Y. Xia, J. Xu *et al.*, *Phys. Rev. C* **91**, 047601 (2015)
- [35] T. Malik, C. Mondal, B. K. Agrawal *et al.*, *Phys. Rev. C* **98**, 064316 (2018), arXiv:1811.09077
- [36] J. Dobaczewski, W. Nazarewicz, and P. G. Reinhard, *J. Phys. G* **41**, 074001 (2014)
- [37] P. G. Reinhard and W. Nazarewicz, *Phys. Rev. C* **81**, 051303(R) (2010)
- [38] J. Piekarewicz, W. C. Chen, and F. J. Fattoyev, *J. Phys. G* **42**, 034018 (2015)
- [39] J. D. McDonnell, N. Schunck, D. Higdon *et al.*, *Phys. Rev. Lett.* **114**, 122501 (2015)
- [40] J. E. Bernhard, P. W. Marcy, C. E. Coleman-Smith *et al.*, *Phys. Rev. C* **91**, 054910 (2015)
- [41] S. Pratt, E. Sangaline, P. Sorensen *et al.*, *Phys. Rev. Lett.* **114**, 202301 (2015)
- [42] W.-J. Xie and B.-A. Li, *Astrophys. J.* **883**, 174 (2019)
- [43] W.-J. Xie and B.-A. Li, *Astrophys. J.* **899**, 4 (2020)
- [44] C. Drischler, R. J. Furnstahl, J. A. Melendez *et al.*, *Phys. Rev. Lett.* **125**, 202702 (2020)
- [45] J. Xu, J. Zhou, Z. Zhang *et al.*, *Phys. Lett. B* **810**, 135820 (2020)
- [46] V. Kejzlar, L. Neufcourt, W. Nazarewicz *et al.*, *J. Phys. G* **47**, 094001 (2020)
- [47] G. F. Bertsch and D. Bingham, *Phys. Rev. Lett.* **119**, 252501 (2017), arXiv:1703.08844
- [48] A. Pastore, *J. Phys. G* **46**, 052001 (2019), arXiv:1810.05585
- [49] A. Tamii, I. Poltoratska, P. Von Neumann-Cosel *et al.*, *Phys. Rev. Lett.* **107**, 062502 (2011)
- [50] X. Roca-Maza, X. Viñas, M. Centelles *et al.*, *Phys. Rev. C* **92**, 064304 (2015)
- [51] S. S. Dietrich and B. L. Berman, *At. Data Nucl. Data Tables* **38**, 199 (1988)
- [52] X. Roca-Maza, M. Brenna, B. K. Agrawal *et al.*, *Phys. Rev. C* **87**, 034301 (2013)
- [53] M. Wang, G. Audi, F. G. Kondev *et al.*, *Chin. Phys. C* **41**, 030003 (2017)
- [54] I. Angeli and K. Marinova, *At. Data Nucl. Data Tables* **99**, 69 (2013)
- [55] D. Patel, U. Garg, M. Fujiwara *et al.*, *Phys. Lett. B* **726**, 178 (2013)
- [56] D. Vautherin and D. M. Brink, *Phys. Rev. C* **5**, 626 (1972)
- [57] L. W. Chen, C. M. Ko, B. A. Li *et al.*, *Phys. Rev. C* **82**, 024321 (2010)
- [58] L.-W. Chen and J.-Z. Gu, *J. Phys. G* **39**, 035104 (2012)
- [59] M. Kortelainen, T. Lesinski, J. Moré *et al.*, *Phys. Rev. C* **82**, 024313 (2010)
- [60] E. Chabanat, P. Bonche, P. Haensel *et al.*, *Nucl. Phys. A* **627**, 710 (1997)
- [61] Z. Zhang and L. W. Chen, *Phys. Rev. C* **92**, 031301(R) (2015)
- [62] G. Colò, L. Cao, N. Van Giai, and L. Capelli, *Comput. Phys. Commun.* **184**, 142 (2013)
- [63] O. Bohigas, A. Lane, and J. Martorell, *Phys. Rep.* **51**, 267 (1979)
- [64] T. Sil, S. Shlomo, B. K. Agrawal, and P.-G. Reinhard, *Phys. Rev. C* **73**, 034316 (2006)
- [65] J. Blaizot, *Phys. Rep.* **64**, 171 (1980)
- [66] A. Bohr and B. Mottelson, *Nuclear Structure, Vols. I and II* (Benjamin, London, 1975)
- [67] X. Roca-Maza, M. Brenna, G. Colò *et al.*, *Phys. Rev. C* **88**, 024316 (2013)
- [68] URL <https://madai.phy.duke.edu>
- [69] C. E. Rasmussen and C. K. I. Williams, *Gaussian Processes for Machine Learning* (MIT Press, Cambridge, MA, 2006)
- [70] M. D. Morris and T. J. Mitchell, *J. Stat. Plan. Inf.* **43**, 381 (1995)
- [71] J. Erler, P. Klüpfel, and P.-G. Reinhard, *J. Phys. G* **37**, 064001 (2010)
- [72] B. G. Carlsson, J. Dobaczewski, and M. Kortelainen, *Phys. Rev. C* **78**, 044326 (2008)
- [73] F. Raimondi, B. G. Carlsson, and J. Dobaczewski, *Phys. Rev. C* **83**, 054311 (2011)
- [74] R. Wang, L. W. Chen, and Y. Zhou, *Phys. Rev. C* **98**, 054618 (2018)